



A comparative study on the reinforcement effect of polyethylene terephthalate composites by inclusion of two types of functionalized graphene

Yuzhou Wang^{1,2} · Zhanbo Wang¹ · Jiahuan Zhu¹ · Hongchuang Li¹ · Zhichao Zhang¹ · Xiang Yu^{1,2}

Received: 3 August 2021 / Accepted: 28 September 2021 / Published online: 11 October 2021
© The Author(s), under exclusive licence to Springer-Verlag GmbH Germany, part of Springer Nature 2021

Abstract

In this paper, graphene oxide (GO) and maleic anhydride–functionalized pristine graphene (MAGN) based on Diels-Alder reaction were synthesized in order to comparatively study the reinforcement effect on the polyethylene terephthalate (PET) composites. PET nanocomposites with GO or MAGN were prepared by a melt-blending method with varying concentrations of nanofillers from 0.05 wt to 0.3 wt%. The structure, the thermal stability, and the mechanical and crystallization properties of the obtained PET composites were systematically investigated by scanning electronic microscopy (SEM), tensile tests, thermo-gravimetric analysis (TGA), differential scanning Calorimetry (DSC), and dynamic mechanical analysis (DMA). The results show that the thermal stability and the mechanical and crystallization properties of PET are improved by GO and MAGN inclusion. When the filler loading was 0.1 wt%, the tensile strength of MAGN/PET and GO/PET was increased by 28.9 % and 11.8% compared with the pure PET, which indicates the MAGN shows a better reinforcement effect on PET nanocomposites. Moreover, the MAGN also acts as a more efficient nucleating agent for PET compared with GO exhibiting higher degrees of crystallinity.

Keywords Polyethylene terephthalate composites · Functionalized graphene · Diels-Alder reaction · Mechanical properties

Introduction

Polyethylene terephthalate (PET) is one of the most comprehensively excellent thermoplastic resin, which has good chemical stability, high processability, and great dimensional stability [1–3]. It is widely used in the field such as fibers, membranes, bottles, and plastics. Often, many of these applications demand higher mechanical strength and heat resistance. Therefore, many efforts were performed to make higher mechanical and thermal properties of PET, and one of the most desirable routes was to add reinforcement

nanofillers into PET matrix, such as graphene (GN) [4], graphene oxide (GO) [5], carbon nanotubes (CNTs) [6], nano-silica [7], and boron nitride nanosheets (BNNs) [1].

Among the above different nanofillers, GN, a new carbon material with a single layer of sp^2 carbon atoms arranged in a honeycomb structure, has drawn wide attention due to its excellent physical and chemical properties, such as high Young's modulus (~1 TPa), great strength (130 GPa), large specific surface area (~2630 $m^2 g^{-1}$) [2], and good thermal conductivity (5000 $W m^{-1} K^{-1}$) [8]. The inclusion of graphene as structural reinforcement fillers is expected to improve matrix-dominated mechanical and thermal properties including strength, Young's modulus, and thermal stability. Bandla and Hanan reported the mechanical properties of PET/GN nanocomposites [9]. Yu et al. have investigated the fabrication of high-strength PET fibers modified with graphene oxide (GO) of varying lateral size [10]. The result shows that the use of small lateral-sized graphene oxide (SGO) yields the best dispersion and interfacial compatibility properties within PET matrix, and the PET/SGO fibers loaded with 0.1 wt% SGO show the highest tensile strength (890 MPa) and Young's modulus (30 GPa).

✉ Yuzhou Wang
wangyuzhoumse@163.com

✉ Xiang Yu

¹ College of Materials Engineering, Henan University of Engineering, Zhengzhou 451191, China

² Henan Key Laboratory of Electronic Ceramic Materials and Application; Henan Engineering Laboratory of Functional Inorganic Nonmetallic Materials, Zhengzhou 451191, China

However, the GO and GN present poor compatibility with most polymer, and the GO and GN sheets tend to aggregate in the polymer matrix. Therefore, chemical functionalization of graphene was performed to solve the problem. Aoyama et al. reported the functionalization of graphene with trimellitic anhydride groups and its effect on melt-mixing graphene with PET in composites [4]. Xing et al. studied the functionalization of GO via a three-step reaction, so that the modified GO can improve the compatibility between GO and PET phases and enhance the thermal stability and crystallization properties of PET [11]. It was mentioned that these methods to strengthen PET composites all chose GO or functionalized GO, because the abundant oxygen-containing functional group on the GO surface can react with other chemical compound easily to grafting many functional groups. Nevertheless, the GO fabrication process is complex and time-consuming along with certain water pollution and danger of explosions. Hence, in order to overcome the disadvantage of GO preparation process, how to directly modify the pristine graphene to increase dispersibility of GN in PET matrix as well as the improved properties of GN/PET nanocomposites needs to further explored.

Recently, the functionalization of graphene based on Diels-Alder (D-A) reaction has attracted many interests [12–14]. The D-A reaction usually occurs between a conjugated diene and a dienophile, in which graphene usually reacts as a diene. Sarkar et al. first reported the successful D-A reaction between graphene and a series of dienophile [15]. Since then, researchers investigated the D-A reaction between pristine graphene and maleic anhydride (MA) [14], maleimide [14], and hexadecyl acrylate [13], et al. Among these dienophiles, MA has good D-A reactive activation.

Inspired by the above facts, in this work, GO and the functionalized pristine graphene were chosen as two structural reinforcement fillers. The functionalized pristine graphene was fabricated based on the solvent-free D-A reaction, in which MA was chosen as the dienophile. The GO/PET and the modified pristine graphene/PET nanocomposites were prepared by melt-blending. The prepared PET nanocomposites were characterized and compared in terms of

their mechanical properties, the crystallinity, and the thermal stability.

Experimental section

Materials

Natural graphite was bought from Qingdao Tengshengda Carbon Machinery Co. Ltd. Pristine graphene was provided by Xiamen Kaina Co. Ltd. Polyethylene terephthalate pellets were obtained from Zhejiang Kingsway HighTech Co., Ltd. Maleic anhydride and potassium bromide were bought from Shanghai Aladdin Chemical Reagent Co., Ltd., China.

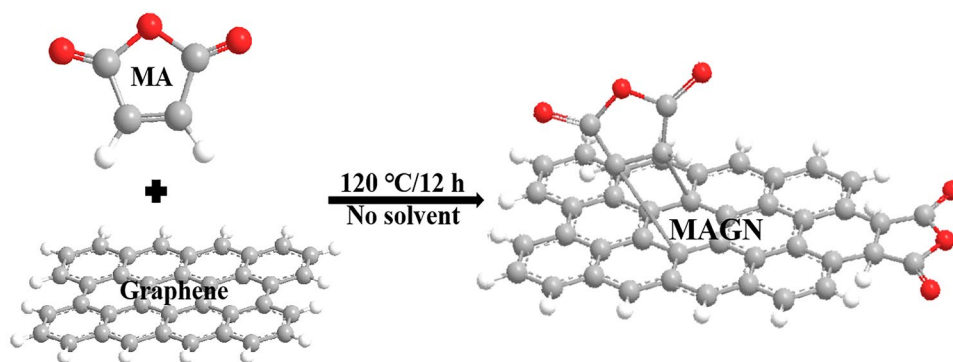
Fabrication of GO and the MAGN

The GO was prepared from natural graphite flakes via a modified Hummer's method, as reported in the previous literature [16]. The preparation of MA-functionalized pristine graphene (MAGN) is based on the D-A reaction. Figure 3 shows the reaction process of graphene functionalization. The reaction was carried out in a three-point round-bottom flask, using graphene and maleic acid with a mass ratio of 1:20. Under the protection of N₂, the slurry was fully reacted at 120 °C for 12 h. The obtained slurry was added to acetone solvent, and the slurry/acetone solution was treated by ultrasonic for 30 min and separated by centrifugation (5000 rpm, 30 min). The obtained black slurry was washed 3 times to remove the unreacted MA molecules, and the final slurry (MAGN) was dried and stored in a vacuum oven for further use. The D-A reaction between pristine graphene and MA is demonstrated in Fig. 1.

Fabrication of GO/PET and GNMA/PET composites

The PET pellets were dried at 130 °C in vacuum for 10 h before use. The GO/PET and GNMA/PET composites were fabricated by melt-blending using a twin screw extruder (Hartec, HTDG-16, China). The nanofiller loading was 0.05,

Fig. 1 Schematic diagram of the preparation of the MAGN



0.1, 0.2, and 0.3 wt%, respectively. The extrusion temperature was set at 270–280 °C, and the extrusion was processed for three times for a better dispersion of fillers within the PET matrix. Finally, the obtained extrudates were pelletized, dried, and then molded to tensile specimens using an injection molding machine (SZS-20, Wuhan Ruiming, Wuhan, China).

Characterization

The functional group structures of graphite, GO, GN, and MAGN were analyzed by Fourier transform infrared spectroscopy (FTIR, Nicolet 6700, USA). The scanning range was 400–4000 cm^{-1} . Raman spectra of graphite, GO, GN, and MAGN were measured by a Raman spectroscope (Xploraplus, Japan), and the using laser wavelength was 633 nm. The morphologies of GO, GN, and MAGN were observed by Transmission electron microscopy (TEM, Hitachi H-800) at 100 kV voltage. The sample dispersion was highly diluted, dropped on the microgrid copper net with ultra-thin carbon film, and fully dried to obtain the TEM samples.

The fracture surface morphologies of PET composites were studied using a scanning electron microscope (SEM, Hitachi S-4800). The tensile strength and Young's modulus of pure PET, GO/PET, and MAGN/PET composites were measured by a universal tensile machine. The tensile speed was set as 50 mm/min, and each sample was tested

ten times and the average value was taken as the final value. The melting and crystallization behaviors of pure PET, GO/PET and MAGN/PET composites were measured by a differential scanning calorimeter (DSC, NETZSCH 200 F3, Germany). Under the protection of N_2 atmosphere, the tested temperature range is 30–300 °C at a rate of 10 °C/min. The thermal gravimetric analysis (TGA) test was carried out with a thermo-gravimetric analyzer (Netzsch STA449F3, Germany). Before the test, the samples were fully dried. TGA tests were under N_2 atmosphere, and the temperature range is 30–800 °C with a heating rate of 10 °C/min. Dynamic mechanical analysis (DMA, NETZSCH DMA 242, Germany) of the samples was performed in a N_2 atmosphere at a heating rate of 3 °C/min and a frequency of 1 Hz.

Results and discussion

Figure 2 shows the FTIR spectra of graphite, GO, GN, and MAGN powder. As shown in Fig. 2, graphite shows a flat curve, which exhibits an almost featureless FTIR spectrum [17]. Compared with graphite, GO shows several characteristic peaks at around 1730 cm^{-1} (C=O stretching), 1680 cm^{-1} (C=C stretching), 1397 cm^{-1} (C–OH stretching), and 1064 (C–O of epoxy stretching) cm^{-1} , respectively [18]. As for GN spectrum, GN shows a feature band at 1576 cm^{-1} corresponding to C=C skeleton of graphene. As shown in Fig. 2, the MAGN shows new peaks at near 1694 and 1263

Fig. 2 FTIR spectra of graphite, GO, GN, and MAGN powder

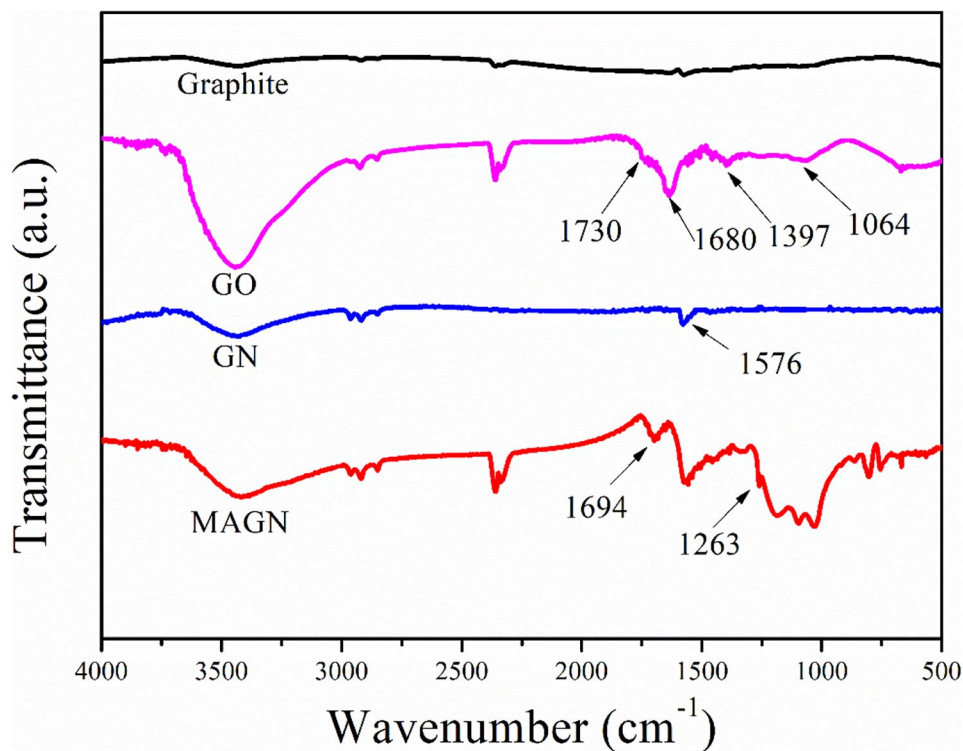
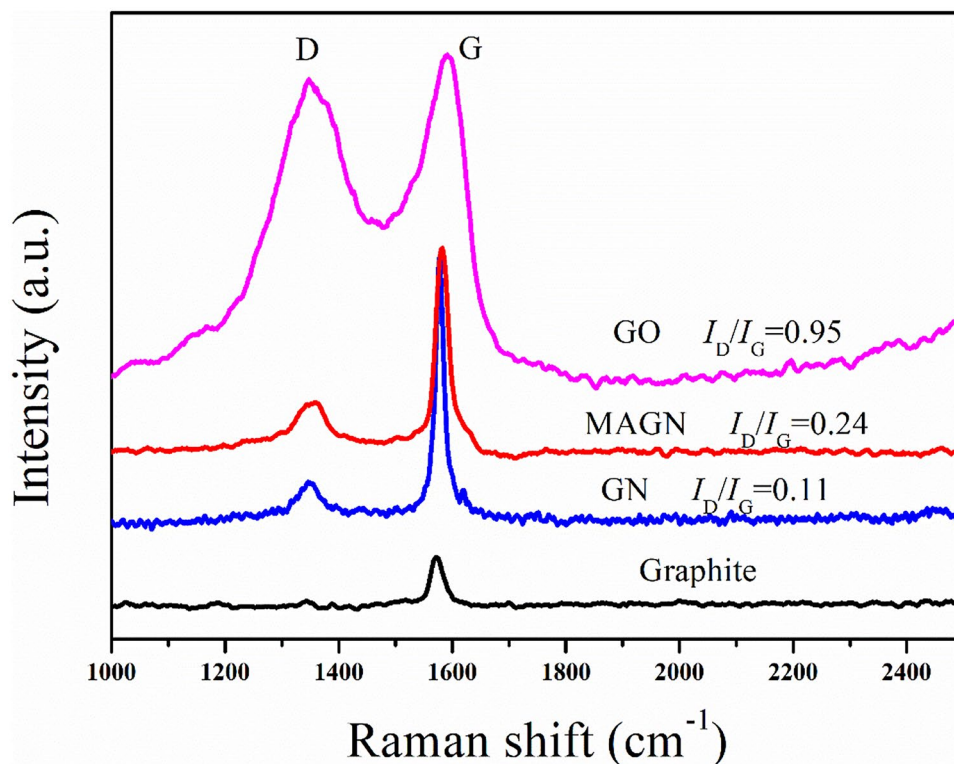


Fig. 3 Raman spectra of graphite, GO, GN, and MAGN powder



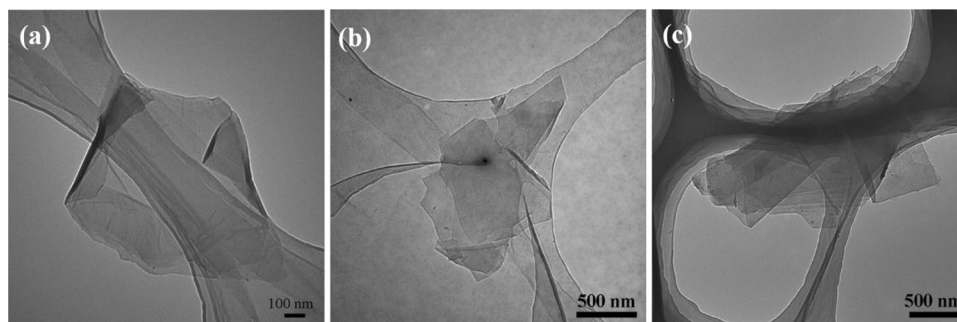
cm^{-1} , which are attributed to C=O and C-O, respectively, indicating the grafting of MA molecules on GN sheets [19]. The FTIR spectra confirms the successful fabrication of GO and MAGN.

Raman spectra of graphite, GO, GN, and MAGN powder are shown in Fig. 3. It is observed that GO, GN, and MAGN show similar peaks at near 1350 and 1580 cm^{-1} , corresponding to D and G bands, respectively. D band is the breathing mode of C- sp^2 atoms in the rings and is related to the disorder presence within the structure, and the G band is the in-plane bond stretching motion of C- sp^2 atoms. The ratio of intensity of D band and G band (I_D/I_G) means the defect degree; the higher value of I_D/I_G means more defects [20]. As shown in Fig. 3, the graphite has no obvious D band, indicating little defects. GO shows a featureless Raman spectrum compared with the literature [18], and the I_D/I_G is 0.95, which suggests the successful preparation of GO.

As for GN, its I_D/I_G value is 0.11; however, after D-A reaction, the I_D/I_G value of MAGN increases to 0.24, and this was attributed to the enhancement in defect concentration because MA molecules was grafted on the graphene surfaces [19]. Moreover, it is noticed that the I_D/I_G value of MAGN was much smaller than that of GO, which suggests that the functionalization-based D-A reaction gives less damage for graphene structure.

TEM micrographs of GO, GN, and MAGN sheets are shown in Fig. 4. It is obvious that few-layer GO structure has been obtained, and the lateral size of GO sheet is around 1.5 μm with a transparent silk-like morphology. Figure 4b shows the TEM micrograph of GN, and the GN also shows transparent and folded structure, which shows typical graphene morphology. Figure 4c reveals the presence of MAGN sheets with lateral dimensions ranging in 1–2 μm . However, compared with GN, the transparency of MAGN becomes

Fig. 4 TEM micrographs of a GO, b GN, and c MAGN



lower, and there were some black dots on the MAGN, which indicate the grafting of MA molecules on MAGN [13]. TEM micrographs suggested the successful fabrication of GO and the D-A reaction between GN and MA molecules.

Figure 5 shows the fracture surfaces morphologies of MAGN/PET and GO/PET composites. As shown in the Fig. 5a, b, when the loading was 0.1 wt%. MAGN and GO can evenly disperse and embedded in the PET matrix. This good adhesion enables the stress on the matrix to be effectively transferred to GO and MAGN. The good dispersion of nanofillers in polymer matrix helps to improve the mechanical strength [10, 21]. When adding more MAGN and GO, the graphene tended to aggregate, as seen in Fig. 5c, d, MAGN and GO occur re-stacking and re-aggregation, which may decrease the tensile strength of PET caused by the stress concentration of MAGN [22, 23]. It is also observed that when the MAGN loading was 0.3 wt%, the MAGN strongly bonded with the PET matrix, which shows a good interaction between nanofillers and polymer matrix.

Figure 6a shows the relationship between tensile strength of PET composites and the filler (GO and MAGN) loadings. As shown in Fig. 6a, when the filler loading was less than 0.1 wt%, the tensile strength of PET composites increased with the filler addition. The highest tensile strength of MAGN/PET and GO/PET was 62.3 and 59.9 MPa, respectively, which was increased by 28.9% and 11.8% compared with the pure PET. When more nanofillers were added to the PET matrix, the tensile strength decreased; this is because the nanofillers occur inevitable aggregation, and this result was consistent with the SEM results (Fig. 5d). Figure 6b shows Young's modulus of PET composites with filler loadings. The Young's modulus of PET composites increased with the filler addition. When the loading is 0.3 wt%, the Young's modulus of the MAGN/PET and GO/PET were 3.90 and 3.49 GPa, respectively, which was increased by 44.4% and 29.3% compared with the pure PET. The reason may be attributed to the interaction between graphene and PET, which limits the motion of the PET chains [24].

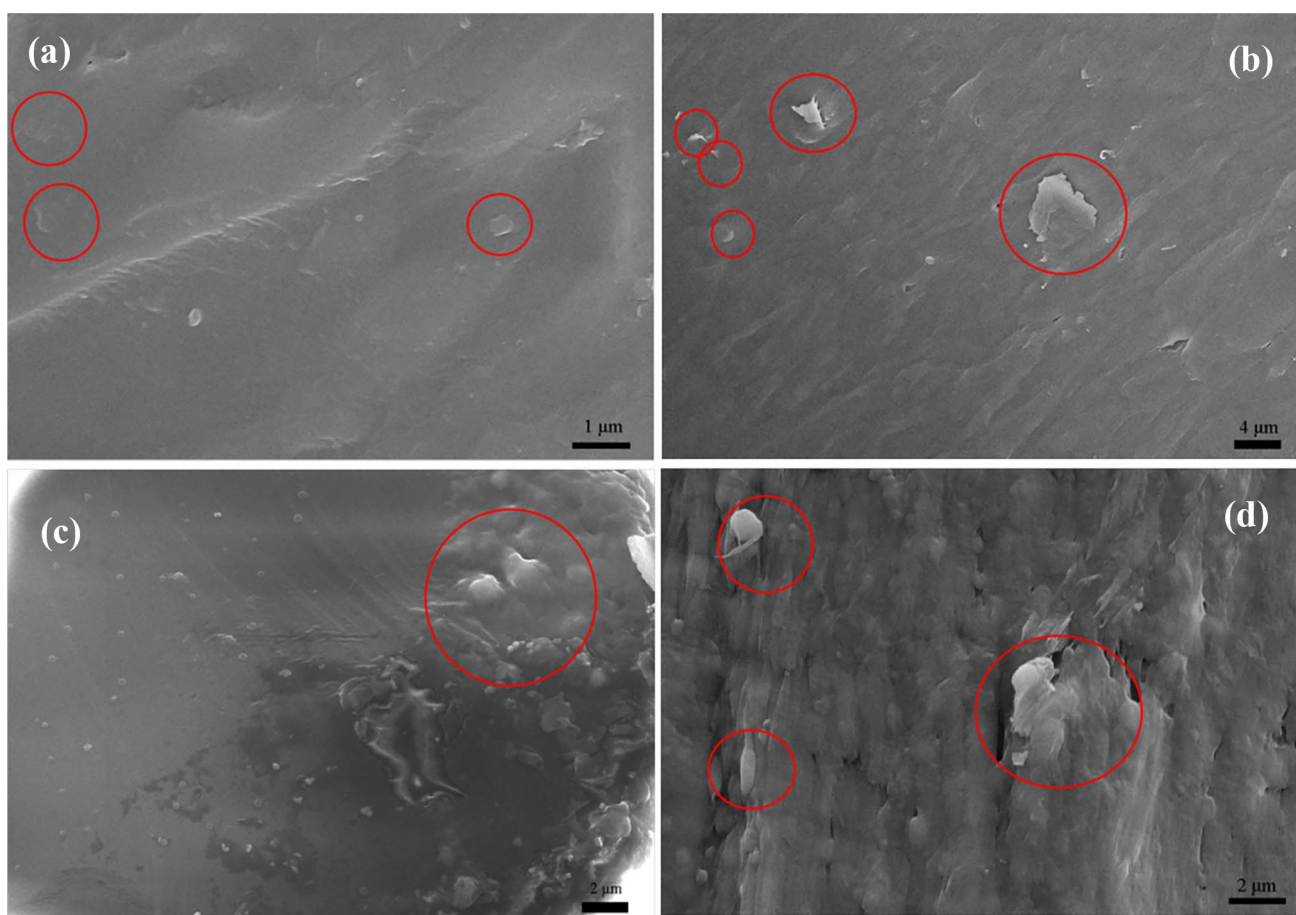


Fig. 5 SEM micrographs of fracture surface of **a** 0.1 wt% MAGN/PET composites, **b** 0.1 wt% GO/PET composites, **c** 0.3 wt% MAGN/PET composites, and **d** 0.3 wt% GO/PET composites

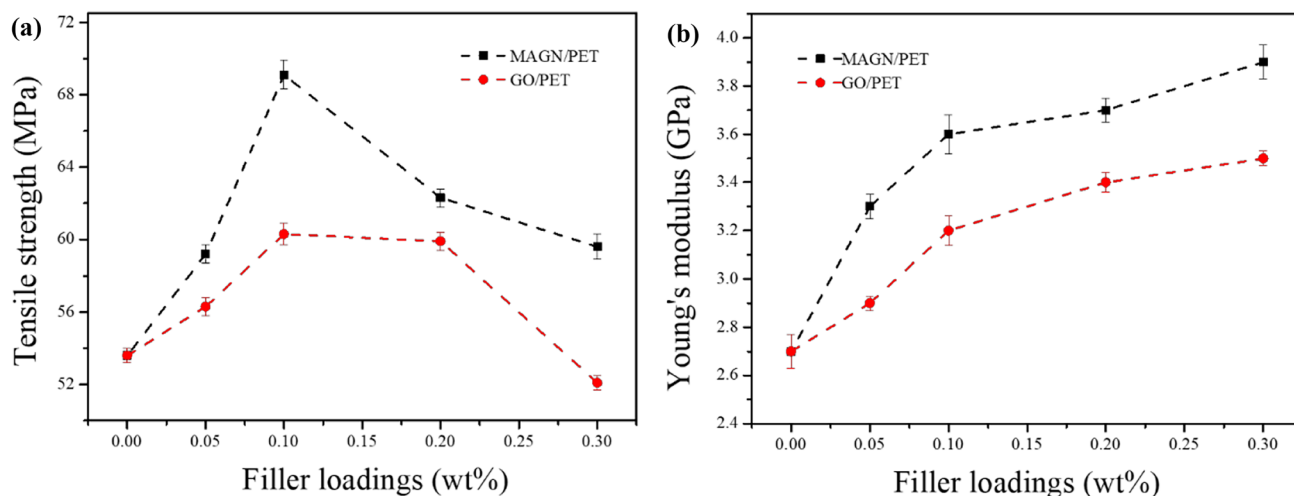


Fig. 6 **a** Tensile strength and **b** Young's modulus of PET composites with filler loadings

The Young's modulus results were in accordance with the previous literatures [16, 17, 19]. In addition, it was observed that the tensile strength and the Young's modulus of MAGN/PET composites were higher than that of GO/PET at the same filler loading, which indicates that MAGN shows a better effect on the reinforcement for PET composites due to the stronger interaction between MAGN and the PET matrix.

Figure 7 shows the DSC melting and cooling curves of pure PET and PET composites and the corresponding DSC data was summarized in Table 1, where T_m , T_c , ΔH_m , and X_c mean melting temperature, crystallization temperature, melting enthalpy, and crystallinity, respectively. The crystallinity of PET and its composites was calculated according to the previous report [10]. It was observed that the

crystallinity and T_c of the PET composites are higher than those of pure PET, because graphene acted as the heterogeneous nucleation agent, which can reduce the energy to form a new crystal plane and improve the crystallization rate [5, 6]. It can be seen from Table 1 that the crystallinity increased first and then decreased with the addition of nanofillers. When the filler loading was more than 0.1 wt%, the X_c value was significantly reduced. This is because too much nanofillers will make graphene agglomerate, resulting in the restrictive movement of PET molecular chains and the formation of incomplete crystals [25, 26]. When filler loading was 0.1 wt%, the crystallinity of PET composite reached the maximum (41.7% for GO/PET and 47.1% for MAGN/PET, respectively). The crystallinity is closely related to the polymer strength. Hence, the DSC results

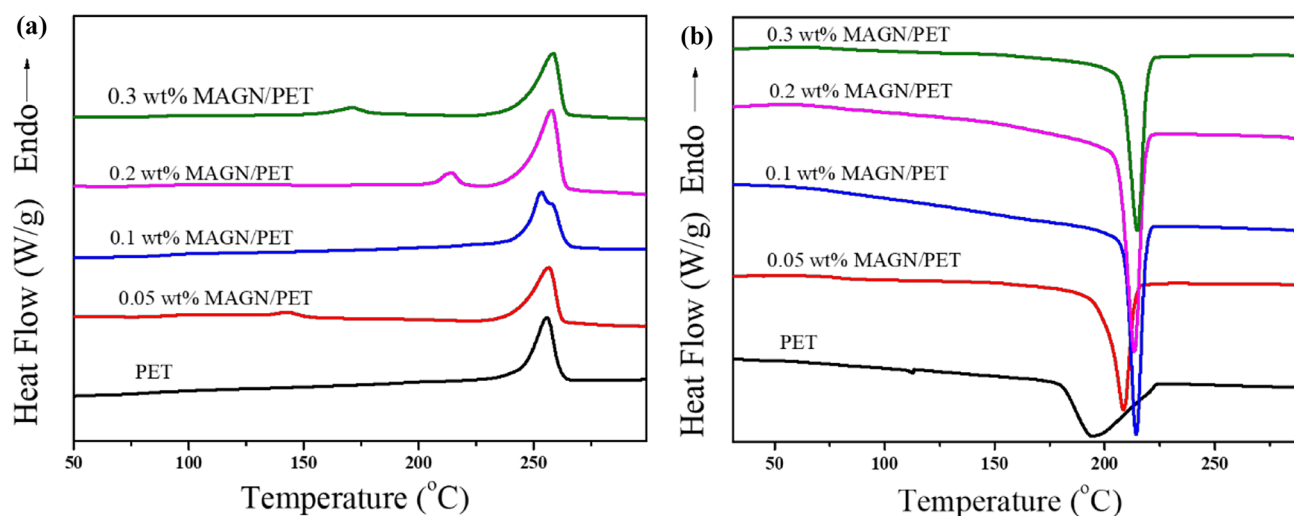


Fig. 7 DSC **a** melting and **b** cooling curves of pure PET and PET composites containing various contents of MAGN

Table 1 DSC data of pure PET and PET nanocomposites

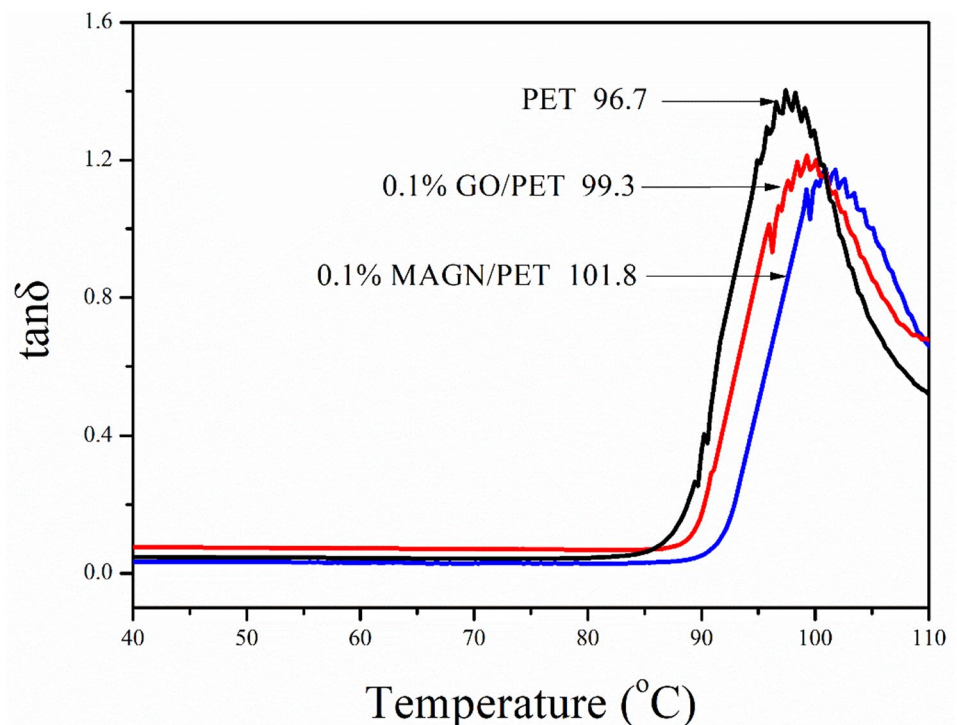
Filler loadings	$T_m/^\circ\text{C}$	$\Delta H_m/\text{J/g}$	$T_g/^\circ\text{C}$	$X_c/\%$
0	255.7	34.7	194.1	27.6
0.05 GO	249.8	41.5	211.7	33.0
0.1 GO	251.1	52.4	215.3	41.7
0.2 GO	258.3	50.9	214.3	41.0
0.3 GO	258.9	39.2	214.7	31.2
0.05 MAGN	256.8	48.8	208.5	38.9
0.1 MAGN	258.6	59.1	216.3	47.1
0.2 MAGN	257.8	50.7	213.4	40.3
0.3 MAGN	258.7	45.2	214.7	40.0

were consistent with the tensile strength results (Fig. 6). Moreover, the X_c value of MAGN/PET was higher than that of GO/PET composites at the same content, indicating that MAGN can lead to a better interface interaction in PET matrix and effectively improve the mechanical properties of the PET composites.

DMA test has a higher sensitivity for determination of the glass transition temperature (T_g); usually, the temperatures corresponding to the $\tan \delta$ peaks can be taken as the T_g [27]. Figure 8 exhibits the $\tan \delta$ curves of pure PET, 0.1 wt% GO/PET, and 0.1 wt% MAGN/PET composites. As shown in Fig. 8, the T_g of pure PET was 96.7; after inclusion of GO or MAGN, the $\tan \delta$ peaks of PET composites shifted toward high temperature. Compared with GO/PET composites, the MAGN/PET composites have a higher T_g value (101.8 °C). The T_g results indicate

that, compared with GO, MAGN has better dispersion and a stronger affinity with the PET matrix. Moreover, as well as known, the $\tan \delta$ value is positively correlated with the amorphous area of the composites [28]. The $\tan \delta$ value decreased markedly with the addition the GO and MAGN, which indicates that the movement of the PET molecular chains was constrained substantially by the fillers [27].

Figure 9 shows the TGA curves of pure PET and its composites, and the TGA data is listed in Table 2. The temperature ($T_{5\%}$) refers to as the initial temperature of thermal decomposition, and the T_{\max} means the temperatures at the maximum rate of mass loss. Both $T_{5\%}$ and T_{\max} are used to estimate the thermal stability of PET [10]. As shown in Fig. 9a, b, MAGN/PET and GO/PET composites have similar thermal decomposition trend with pure PET, but the inclusion of GO and MAGN can improve the thermal stability of PET. As shown in Table 2, the $T_{5\%}$ and T_{\max} of the MAGN/PET are higher than that of GO/PET, which indicates the better thermal stability. This is due to the improvement of dispersion and compatibility of graphene functionalized by maleic anhydride, which can improve the interfacial interaction between PET and polymer [25]. During the decomposition process, many degradation products were adsorbed by graphene, which slowed down the decomposition process of PET matrix [29]. The thermal decomposition temperature of PET containing 0.1 wt% MAGN increased about 8 °C compared with that of pure PET.

Fig. 8 Loss tangent ($\tan \delta$) curves of pure PET, GO/PET, and MAGN/PET composites

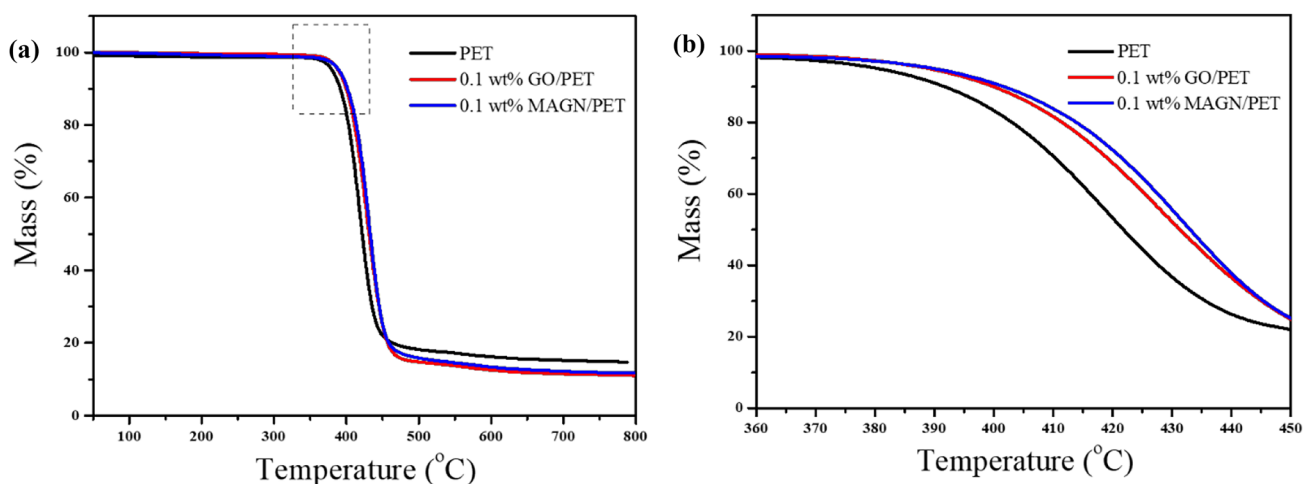


Fig. 9 **a** TGA curves of pure PET, 0.1 wt% GO/PET, and 0.1 wt% MAGN/PET composites and **b** local enlargement of TGA curves

Table 2 TGA data of pure PET and PET nanocomposites

Sample	$T_{5\%}/^{\circ}\text{C}$	$T_{\text{max}}/^{\circ}\text{C}$
PET	394.7	423.5
0.1 wt% GO/PET	401.8	429.3
0.1 wt% MAGN/PET	406.3	430.7

Conclusion

In this paper, a green strategy to significantly enhance thermal stability, mechanical, and crystallization properties of PET was demonstrated. GO was prepared by a hummer's method, and the functionalized graphene was synthesized via a D-A reaction between MA and pristine graphene. The influence of GO and MAGN on the mechanical and thermal properties of PET nanocomposites has been studied. Enhanced mechanical properties were investigated by tensile tests, and the results show when the filler loading was 0.1 wt%; the tensile strength of MAGN/PET and GO/PET was increased by 28.9% and 11.8% compared with the pure PET, which indicates that the MAGN shows a better reinforcement effect on PET composites. In addition, the MAGN/PET and GO/PET composites can exhibit better improvement in crystallinity and thermal stability even at lower filler loading (0.1 wt%), ensuring strong interaction between graphene and the polymer matrix. Finally, all the results suggest that, compared with GO, the MAGN obtained by green D-A reaction exhibits a more efficient improvement for properties of PET nanocomposites.

Author contribution All authors contributed to the study conception and design. Material preparation, data collection, and analysis were performed by Zhanbo Wang, Jiahuan Zhu, Hongchuang Li,

and Zhichao Zhang. The first draft of the manuscript was written by Yuzhou Wang. The manuscript was revised by Xiang Yu.

Declarations

Conflict of interest The authors declare no competing interests.

References

- Sahoo A, Gayathri HN, Sai TP, Upasani PS, Raju V, Berkman J, Ghosh A (2020) Enhancement of thermal and mechanical properties of few layer boron nitride reinforced PET composite. *Nanotechnology* 31:315706
- Ma J, Yu L, Chen S, Chen W, Wang Y, Guang S, Zhang X, Lu W, Wang Y, Bao J (2019) Structure–property evolution of poly(ethylene terephthalate) fibers in industrialized process under complex coupling of stress and temperature field. *Macromolecules* 52:565–574
- Gorrasi G, Bugatti V, Milone C, Mastrorlando E, Piperopoulos E, Iemmo L, Bartolomeo AD (2018) Effect of temperature and morphology on the electrical properties of PET/conductive nanofillers composites. *Compos Part B Eng* 135:149–154
- Aoyama S, Ismail I, Yong TP, Macosko CW, Ougizawa T (2020) PET/Graphene compatibilization for different aspect ratio graphenes via trimellitic anhydride functionalization. *ACS Omega* 5:3228–3239
- Awad SA, Khalaf EM (2018) Improvement of the chemical, thermal, mechanical and morphological properties of polyethylene terephthalate–graphene particle composites. *B Mater Sci* 41:67–73
- Rodríguez-Uicab O, May-Pat A, Avilés F, Toro P, Yazdani-Pedram M (2013) Influence of processing method on the mechanical and electrical properties of MWCNT/PET composites. *J Mater Sci* 2:656372
- Behzadian R, Shahrajabian H (2019) Experimental study of the effect of nano-silica on the mechanical properties of concrete/pet composites. *Ksce J Civ Eng* 23:3660–3668
- Li Z, Liu Z, Sun HY, Gao C (2015) Superstructured assembly of nanocarbons: fullerenes, nanotubes, and graphene. *Chem Rev* 115:7046–7117

9. Bandla S, Hanan JC (2012) Microstructure and elastic tensile behavior of polyethylene terephthalate-exfoliated graphene nanocomposites. *J Mater Sci* 47:876–882
10. Yu W, Zhang X, Gao X, Liu H, Zhang X (2020) Fabrication of high-strength PET fibers modified with graphene oxide of varying lateral size. *J Mater Sci* 55:8940–8953
11. Xing L, Yao W, Wang S, Zhang Y, Mao S, Wang G, Liu J, Huang L, Li H, Belfiore LA, Tang J (2018) Effects of modified graphene oxide on thermal and crystallization properties of PET. *Polymers* 10:613
12. Fort EH, Donovan PM, Scott LT (2009) Diels-alder reactivity of polycyclic aromatic hydrocarbon bay regions: implications for metal-free growth of single-chirality carbon nanotubes. *J Am Chem Soc* 131:16006–16007
13. Cao RR, Wang YZ, Chen S, Han N, Liu H, Zhang X (2019) Multiresponsive shape-stabilized hexadecyl acrylate-grafted graphene as a phase change material with enhanced thermal and electrical conductivities. *ACS Appl Mater Interfaces* 11:8982–8991
14. Seo JM, Jeon IY, Baek JB (2013) Mechanochemically driven solid-state Diels-Alder reaction of graphite into graphene nanoplatelets. *Chem Sci* 4:4273–4277
15. Sarkar S, Bekyarova E, Niyogi S, Haddon RC (2011) Diels-Alder chemistry of graphite and graphene: graphene as diene and dienophile. *J Am Chem Soc* 133:3324–3327
16. Liu H, Hou L, Peng W, Zhang Q, Zhang X (2012) Fabrication and characterization of polyamide 6-functionalized graphene nanocomposite fiber. *J Mater Sci* 47:8052–8060
17. Wang Y, Zhang X, Liu H, Zhang X (2019) SMA-Assisted exfoliation of graphite by microfluidization for efficient and large-scale production of high-quality graphene. *Nanomaterials* 9:1653
18. Wang T, Jing LC, Zhu QX, Anita SE, Tian Y, Zhao H, Yuan XT, Wen JG, Li LK, Geng HZ (2020) Fabrication of architectural structured polydopamine-functionalized reduced graphene oxide/carbon nanotube/PEDOT:PSS nanocomposites as flexible transparent electrodes for oleds. *Appl Surf Sci* 500:143997
19. Zabihi O, Ahmadi M, Abdollahi T, Nikafshar S, Naebe M (2017) Collision-induced activation: towards industrially scalable approach to graphite nanoplatelets functionalization for superior polymer nanocomposites. *Sci Rep* 7:3560–3572
20. Wang YZ, Chen T, Gao XF, Liu HH, Zhang XX (2017) Liquid phase exfoliation of graphite into few-layer graphene by sonication and microfluidization. *Mater Express* 7:491–499
21. Ozdemir E, Arenas DR, Kelly NL, Hann JV, Rijswijk BV, Degirmenci V, McNally T (2020) Ethylene methyl acrylate copolymer assisted dispersion of few-layer graphene nanoplatelets in poly (ethylene terephthalate) 205:122836
22. Kim J, Oh J, Lee KY, Jung I, Park M (2017) Dispersion of graphene based nanocarbon fillers in polyamide 66 by dry processing and its effect on mechanical properties. *Compos B Eng* 114:445–456
23. Thayumanavana N, Tambe P, Joshi G (2015) Effect of surfactant and sodium alginate modification of graphene on the mechanical and thermal properties of polyvinyl alcohol (PVA) nanocomposites. *Cellul Chem Technol* 49:69–80
24. Hou WJ, Tang BQ, Lu LL, Sun J, Wang JJ, Qin CX, Dai LX (2014) Preparation and physico-mechanical properties of amine-functionalized graphene/polyamide 6 nanocomposite fiber as a high performance material. *RSC Adv* 4:4848–4855
25. Wang YZ, Gao XF, Liu HH, Zhang J, Zhang XX (2020) Green fabrication of functionalized graphene via one-step method and its reinforcement for polyamide 66 fibers. *Mater Chem Phys* 240:122288
26. Stanciu MD, Draghicescu HT, Tamas F, Terciu OM (2020) Mechanical and rheological behaviour of composites reinforced with natural fibres. *Polymers* 12:1402
27. Zhang J, Gao XF, Zhang XY, Liu HH, Zhang H, Zhang XX (2019) Polyamide 66 and amino-functionalized multi-walled carbon nanotube composites and their melt-spun fiber. *J Mater Sci* 54:11056–11068
28. Filho FCG, Luz FS, Oliveira MS, Pereira AC, Costa UO, Monteiro SN (2020) Thermal behavior of graphene oxide-coated piassava fiber and their epoxy composites. *J Mater Res Technol* 9:5343–5351
29. Azman NFI, Zuhairi SA, Ratnam CT, Yaakob Y, Mama MS (2021) Incorporation of multiwalled carbon nanotubes and graphene nanoplatelets on the morphology and properties of polyethylene terephthalate nanocomposites. *J Nanomater* 1:1–9

Publisher's Note Springer Nature remains neutral with regard to jurisdictional claims in published maps and institutional affiliations.